Concentration, temporal variation and sources of black carbon in the Mount Everest region retrieved by real-time observation and simulation

Xintong Chen [1, 4], Shichang Kang [1, 2, 4], Zhiyuan Cong[2, 3], Junhua Yang [1], Yaoming Ma [3]

[1]State Key Laboratory of Cryospheric Science, Northwest Institute of Eco-Environment and Resources, Chinese Academy of Sciences, Lanzhou 730000, China

[2]CAS Center for Excellence in Tibetan Plateau Earth Sciences, Chinese Academy of Sciences, Beijing 100101, China

[3]Key Laboratory of Tibetan Environment Changes and Land Surface Processes, Institute of Tibetan Plateau Research, Chinese Academy of Sciences, Beijing 100101, China

[4]University of Chinese Academy of Sciences, Beijing 100049, China

Correspondence to: Shichang Kang (shichang.kang@lzb.ac.cn)

Abstract. Based on the high-resolution measurement of black carbon (BC) at Qomolangma (Mt. Everest) Station (QOMS, 28.36°N, 86.95°E, 4276 m a.s.l.) from 15 May 2015 to 31 May 2017, we investigated the seasonal and diurnal variations in BC and its potential source regions. Monthly and daily mean BC concentrations reached the highest values in the pre-monsoon season, which were at least one magnitude higher than the lowest values in the monsoon season. For the diurnal variation, the BC concentrations remained significantly high from midnight to noon in the pre-monsoon season. Meanwhile, the westerly winds prevailed during this period, implying the potential for pollutants to be transported across the Himalayas from long-distance sources to QOMS along the valley. In the monsoon season, the BC concentrations remained low but peaked in the morning and in the afternoon, which might be caused by local emissions from cooking. By analyzing the simulation results from the backward trajectories of air masses and the fire spot distribution from the MODIS data, we found that the seasonal cycle of BC was significantly influenced by the atmospheric circulation and combustion intensity in the Mt. Everest region. The transport mechanisms of BC were further revealed using a WRF-Chem simulation during severe pollution episodes. For the pollution event in the monsoon season, BC aerosols in South Asia were uplifted and transported to the Mt. Everest region by the southerly winds in the upper atmosphere. However, for the events in the pre-monsoon season, BC from northern India was transported and concentrated on the southern slope of the Himalayas by the northwesterly winds in the lower atmosphere and then transported across the Himalayas by the mountain-valley wind. Relatively less BC from northwestern India and Central Asia was transported to the Mt. Everest region by the westerly winds in the upper atmosphere.

1 Introduction

Black Carbon (BC), mainly from the incomplete combustion of fossil fuels or biomass, has drawn much attention due to its influences on the environment and human health (Bond, 2004; Ramanathan et al., 2005; Anenberg et al., 2012) and is seen as an important factor that may lead to global warming, in addition to greenhouse gases (Hansen et al., 2000; Jacobson, 2002; Bond et al., 2013; Ramanathan and Carmichael, 2008). BC can substantially absorb solar radiation and causes atmospheric

32 heating (Jacobson, 2001; Ramanathan et al., 2005; Ji et al., 2015). Moreover, BC can be suspended as fine particles in the

33 atmosphere for approximately one week, be transported far away from its emission sources, and then be removed by dry and

34 wet deposition (Oshima et al., 2012; Cooke et al., 2002; Jurado et al., 2008). When BC is deposited on snow and ice, it can

35 significantly reduce surface albedo (Flanner et al., 2007; He et al., 2017) and accelerate glacier and snow cover melting,

36 causing an impact on the regional climate, hydrology, and water resources (Li et al., 2018; Ming et al., 2008; Ramanathan and

37 Carmichael, 2008).

38   The Tibetan Plateau (TP), generally known as the "Third Pole", is the highest plateau with a large number of glaciers and

39 snow cover (Kang et al., 2010; Lu et al., 2010; Yao et al., 2012). Even though the TP is a remote region with few affects from

40 anthropogenic activities, previous observations have indicated that BC is an important contributor to the rapid shrinking of

41 glaciers over the TP via decreasing surface albedo and atmospheric warming (Xu et al., 2009; Yang et al., 2015; Li et al., 2017b;

42 Zhang et al., 2017b; Qu et al., 2014; Ji, 2016; Xu et al., 2016; Lee et al., 2017). Moreover, previous studies have also suggested

43 that the emissions from South Asia and East Asia are the major sources of BC on the TP (Li et al., 2016a; Lu et al., 2012; He

44 et al., 2014b; Zhang et al., 2015; Yang et al., 2018), and the high emissions from South Asia can be transported across the

45 Himalayas and further to the inland TP (Luthi et al., 2015; Xu et al., 2014; Cong et al., 2015a; Kang et al., 2016; Wan et al.,

46 2015). Meanwhile, the seasonality of BC aerosols is closely related to atmospheric circulation that helps to bring the BC

47 aerosols across the Himalayas (Cong et al., 2015a; Cong et al., 2015b; Yang et al., 2018). Additionally, a large number of

48 studies have demonstrated that the BC and dust from Central Asia and northern Africa could also be transported to the TP

49 (Wang et al., 2016; Lu et al., 2012; Zhao et al., 2012; Wu et al., 2010; Zhang et al., 2015).

50   Mt. Everest could be regarded as a very sensitive area under the influence of BC aerosols. Previous research on

51 atmospheric BC in the Mt. Everest region was mainly based on the thermal/optical analytical method, using quartz filter

52 samples (Cong et al., 2015a). However, there is still a lack of investigations on the diurnal and seasonal variations in BC in

53 this region. Therefore, to fill such gaps and understand the variations in and sources of BC in the pristine region, there is a

54 need for an efficient approach and additional studies. The aethalometer can provide real-time high-resolution observation data

55 on the BC concentration, which is very important and necessary to better depict the characteristics of BC and its effects on the

56 environmental change.

57   In comparison with the observations, numerical models can better represent the atmospheric physical and chemical

58 processes. Many studies have used global climate models (GCMs) and chemical transport models (CTMs) to investigate the

59 origin and transportation of BC over the TP (Lu et al., 2012; Zhang et al., 2015; Menon et al., 2010; Kopacz et al., 2011; He

60 et al., 2014a). However, due to the coarse resolution, it is difficult for the CTMs and GCMs to capture the surface details of

61 the TP (Ji et al., 2015; Gao et al., 2008). Regional climate models (RCMs) can compensate for the shortcomings of coarser

62 global model grids by high-resolution simulations. In recent decades, RCMs have been developed to include multiple modules

63 and atmospheric chemistry processes. In addition, the advanced regional climate-chemistry model, Weather Research and

2

Forecasting (WRF) model (Skamarock et al., 2005) coupled with chemistry (WRF-Chem) has been successfully applied for air quality research on the TP (Yang et al., 2017; Yang et al., 2018).

Here, we present real-time data of the BC concentration measured by the new Aethalometer model AE-33 from 15 May 2015 to 31 May 2017. The observed results are used to characterize the temporal variation and provide important information on the possible sources and transport mechanisms of BC. By combining high-resolution measurements of the BC concentration and the WRF-Chem model, we investigated the concentration level, temporal variation, and sources of BC in the Mt. Everest region. The purpose of this study is to understand the impact of trans-boundary atmospheric BC on the Mt. Everest region and depict the transport pathways of BC at different spatiotemporal scales.

2 Materials and methods

2.1 Sampling site and meteorological conditions

Mt. Everest (27.98°N, 86.92°E, 8844 m a.s.l.), the summit of the world, is located in the central Himalayas. The southern slope of Mt. Everest is adjacent to the Indian continent, and the climate is warm and humid under the influence of the Indian summer monsoon. Conversely, the northern side is cold and dry since the warm and humid airflow cannot reach it. Qomolangma (Mt. Everest) Station for Atmospheric and Environmental Observation and Research, Chinese Academy of Sciences (QOMS, 28.36°N, 86.95°E, 4276 m a.s.l.) (Fig. 1) is located on the northern slope of Mt. Everest, which was established for continuous monitoring of the atmospheric environment (Cong et al., 2015a; Ma et al., 2011).

The meteorological parameters, i.e., air temperature, air pressure, humidity, wind speeds and wind direction, were recorded by an automatic weather station at QOMS with 10 min time intervals. Meanwhile, the precipitation data were collected by artificial measurement, as shown in Fig. S1. The entire year was divided into four seasons according to the Indian monsoon transition characteristics, which includes pre-monsoon (March to May), monsoon (June to September), post-monsoon (October to November), and winter (December to February) (Praveen et al., 2012; Zhang et al., 2017a). A clear seasonal cycle of temperature and humidity can be observed in Fig. S1. Specifically, the temperature was high during the monsoon season and low during winter, with a maximum in July and a minimum in January. Humidity followed a similar trend, with high values from late July to early August and low values from December to February. During the observation period, the wind speed increased significantly from November to April. The wind direction at QOMS is affected by the local topography, which consists of a series of small valleys. During the pre-monsoon season (dry period), the westerly and southerly winds begin to develop and play an important role in atmospheric pollution circulation. However, during the monsoon season, the southwesterly winds prevail and bring much moisture from the Indian Ocean to the Mt. Everest region, increasing the humidity and precipitation. With the retreat of the monsoon, the southwesterly winds decrease and the prevailing wind direction changes to westerly and northeasterly in winter with limited moisture (Fig. S1).

2.2 BC measurements

There are several available methods capable of measuring BC concentrations, and these methods can be classified into three categories. First is the thermal/optical method, which uses a quartz filter to collect aerosols, and they are thermally volatilized in several temperature steps (Schauer et al., 2003). The signals of evolving carbon measured by thermal/optical transmission (TOT) or thermal/optical reflectance (TOR) can be converted to the concentration of BC (Chow et al., 1993; Chow et al., 2001). However, the time difference between sampling and detection, the impact of mineral dust, and the determination of the split between organic carbon (OC) and elemental carbon (EC, the same as BC) can cause deviations (Li et al., 2017a; Schauer et al., 2003). The second category is the technique of the single particle soot photometer (SP2), which can quantify BC by laser-induced incandescence because BC is the predominant refractory absorbing aerosol, which can be heated by an intense laser beam and emit significant thermal radiation (Stephens et al., 2003). This method measures the mass of BC in individual particles, but the accuracy depends on the selected calibration material (Schwarz et al., 2010; Laborde et al., 2012). Finally, the optical method measures the reduction in light intensity induced by BC aerosols collected on the sampling medium (Hansen et al., 1984; Petzold and Schonlinner, 2004). The Aethalometer is a widely used instrument based on the optical method that can provide real-time BC concentration measurements, but all filter-based optical methods exhibit loading effects that can lead to the underestimation of BC concentrations (Bond et al., 1999; Virkkula et al., 2007; Park et al., 2010; Hyvarinen et al., 2013; Drinovec et al., 2015). However, the newly developed Aethalometer model AE-33 uses a real-time loading effect compensation algorithm that can provide high-quality data, which is very helpful for the accurate determination of BC concentrations and source apportionment (Drinovec et al., 2015).

Therefore, the airborne BC concentrations at QOMS were monitored by the new Aethalometer model AE-33 (Magee Scientific Corporation, USA). The instrument was set in an indoor room with an inlet installed at approximately 3 m above the ground level and was operated at an airflow rate of 4 LPM with a 1 min time resolution. AE-33 has seven fixed wavelengths (i.e., 370, 470, 520, 590, 660, 880 and 950 nm), which can acquire the BC concentration according to the light absorption and attenuation characteristics from the different wavelengths (Hansen et al., 1984; Drinovec et al., 2015). Generally, the BC concentration measured at 880 nm is used as the actual BC concentration in the atmosphere, as the absorption of other species of aerosols is greatly reduced in this wavelength (Sandradewi et al., 2008a; Sandradewi et al., 2008b; Fialho et al., 2005; Yang et al., 2009; Drinovec et al., 2015). Compared to previous Aethalometer models, AE-33 uses dual-spot measurement and a real-time calculation of the "loading compensation parameter", which can compensate for the "spot loading effect" and obtain high-quality BC concentration (Drinovec et al., 2015). The main structure of this algorithm is as follows:

$$BC \text{ (reported)} = BC(\text{zero loading}) \times (1 - k\text{ATN}) \qquad (1)$$

$$ATN = -100 \ln(I / I_0) \qquad (2)$$

$$BC1 = BC \times (1 - k\text{ATN1}) \qquad (3)$$

4

125   BC2=BC×(1 − kATN2)   (4)

126   where BC (reported) is the uncompensated BC concentration; BC (zero loading) is the desired ambient BC value that would

127   be obtained in the absence of any loading effect; k is the loading effect compensation parameter; I and I_0 are the light intensity

128   of the measurement spot and reference spot; and ATN is the attenuation of light through filter tape. The BC component of the

129   aerosols is analyzed on two parallel spots drawn from the same input stream in AE-33 but collected at different rates of

130   accumulation. This means that we can obtain different ATN but the same loading parameter k (Drinovec et al., 2015).

131   Combining Eq. (3) and Eq. (4), the compensation parameter k and the desired value of BC compensated back to zero loading

132   can be calculated. Based on the dual-spot technology, the new real-time compensation algorithm allows extrapolation to zero

133   loading and obtains the accurate BC concentration (Drinovec et al., 2015; Crenn et al., 2015; Zhu et al., 2017). Previous studies

134   have evaluated the real-time compensation algorithm of dual-spot Aethalometer model AE-33 and indicated that AE-33 agrees

135   well with the post-processed loading effect compensated data obtained using earlier Aethalometer models and other filter-

136   based absorption photometers, implying the good performance of this new algorithm (Drinovec et al., 2015; Rajesh and

137   Ramachandran, 2018).

2.3 Model simulation and datasets

139   WRF-Chem version 3.6 was used to analyze the spatial distribution, transport mechanism, and source apportionment of

140   BC during the four observed pollution episodes. The WRF-Chem model is an expansion of the WRF meteorological model

141   and considers complex physical and chemical processes such as emission and deposition, advection and diffusion, gaseous and

142   aqueous chemical transformation, and aerosol chemistry and dynamics (Grell et al., 2005). Here, the numerical experiments

143   were performed at a 25 km horizontal resolution with 122 and 101 grid cells in the west-east and north-south directions,

144   respectively. The simulated domain was centered at 25°N, 82.5°E and had a 30-layer structure with the top pressure of 50 hPa.

145   The key physical and chemical parameterization options for the WRF-Chem model were based on a previous study on the TP

146   (Yang et al., 2018). The initial meteorological fields were taken from the National Centers for Environmental Prediction (NECP)

147   reanalysis data with a horizontal resolution of 1° × 1° at 6 h time intervals. The anthropogenic emission inventory was obtained

148   from the Intercontinental Chemical Transport Experiment-Phase B (INTEX-B) (Zhang et al., 2009) with a resolution of 0.5°

149   × 0.5°. The biogenic emissions were obtained from the Model of Emission of Gases and Aerosol from Nature (MEGAN)

150   (Guenther et al., 2006), and the fire emissions inventory was based on the fire inventory from NCAR (FINN) (Wiedinmyer et

151   al., 2011). Additionally, the Model for Ozone and Related chemical Tracers (MOZART, http://www.acom.ucar.edu/wrf-

152   chem/mozart.shtml) (Emmons et al., 2010) dataset was used to create improved initial and boundary conditions for the BC

153   simulations during these pollution episodes.

154   Furthermore, to predict the source region of BC, we used the Hybrid Single-Particle Lagrangian Integrated Trajectory

155   (HYSPLIT-4) model to calculate the backward trajectories of the air masses (Stein et al., 2015), and the calculation data was

obtained from the National Centers for Environmental Prediction/National Center for Atmospheric Research (NCEP/NCAR) reanalysis data (2.5° × 2.5°). The parameter settings for the backward trajectory calculation in the HYSPLIT model were chosen according to a previous study in this area (Xu et al., 2014). The active fire product provided by the Fire Information for Resource Management System (FIRMS, https://firms.modaps.eosdis.nasa.gov/firemap/) was chosen to investigate the biomass burning emissions over the region in different seasons.

3. Results and discussion

3.1 Temporal variations in BC

3.1.1 Monthly variation in BC

The monthly mean BC concentrations at QOMS are shown in Fig. 2a. There was a significant increase in the BC concentrations in winter, and the highest value occurred during the pre-monsoon season (923.1 ± 685.8 ng/m^3 in April). Meanwhile, during the monsoon, lower BC concentrations were recorded, and the lowest value was observed in July (88.5 ± 29.8 ng/m^3). This seasonal change was consistent with the previous studies of elemental carbon (EC or BC) at Nepal Climate Observatory-Pyramid station (NCO-P, 27.95°N, 86.82°E, 5079 m a.s.l.) from March 2006 to February 2008 (Fig. 2b) (Marinoni et al., 2010) and at QOMS from August 2009 to July 2010 (Fig. 2c) (Cong et al., 2015a), indicating a similar BC source between the southern and northern sides of the Himalayas. As EC was sampled by quartz filters and detected using the thermal/optical analytical method in previous studies, there may be some differences in the values of EC compared to those of BC, for instance, the overestimation of EC due to the potential effect of carbonates in mineral dust of the samples when using the thermal/optical method (Li et al., 2017a). The monthly variation in EC at Nam Co Monitoring and Research Station for Multisphere Interactions (Nam Co station, 30.46°N, 90.59°E, 4730 m a.s.l.) from January to December during 2012 (Fig. 2d) (Wan et al., 2015) also showed a similar variation, but the peak value of EC occurred in winter. Additionally, the monthly mean EC concentrations at Nam Co station were generally lower than those at QOMS, suggesting that the impact of the anthropogenic activities on the inland TP was weaker than that on the south edge of the TP. Previous studies have demonstrated that the influence of polluted air masses from the "Atmospheric Brown Clouds" over South Asia could reach the southern foothills of the Himalayas and that the mountain-valley breeze circulation carried the polluted air masses onto the TP (Luthi et al., 2015; Cong et al., 2015a; Bonasoni et al., 2008; Yang et al., 2018). Therefore, the seasonal cycle of BC concentrations at QOMS was likely affected by the atmospheric circulation and the emissions from South Asia, which will be further explained in Section 3.3.

3.1.2 Daily variation in BC

Fig. 3 shows the daily mean BC concentrations at QOMS, which present a significant seasonal pattern, with a maximum

185 during the pre-monsoon season (2772.3 ng/m^3) and a minimum during the monsoon season (36.4 ng/m^3). During the monsoon

186 season, the BC concentration was observed to be lower than 150 ng/m^3, but it gradually increased during the post-monsoon

187 and winter. The mean concentration of daily BC at QOMS was 298.8 ± 341.3 ng/m^3, which was close to the previous result

188 (250 ± 220 ng/m^3) (Cong et al., 2015a).

189 The comparison between daily mean BC concentrations (Fig. 3) and the meteorological parameters (Fig. S1) suggested

190 that the increasing precipitation during the monsoon led to the washout of atmospheric particles, promoting the wet deposition

191 of BC. This process caused a decrease in BC concentrations during the monsoon, representing the background level during the

192 period. The prevailing wind direction was southwesterly during the monsoon period and westerly during the non-monsoon

193 periods. Therefore, the variations in BC might be linked to the influence of meteorological conditions and the contribution of

194 long-distance transport from urbanized areas to QOMS. Moreover, it cannot be ignored that there were continuous high

195 concentrations of BC above 1000 ng/m^3 during 8-10 June 2015, 19-22 March 2016, 9-30 April 2016, and 11-14 April 2017,

196 indicating that the heavy pollution episodes happened at QOMS during those days. A detailed analysis of these pollution events

197 is presented in Section 3.4.

3.1.3 Diurnal variation in BC

199 Diurnal variation characteristics can be used to analyze the impact of local meteorological processes and anthropogenic

200 activities on the BC concentrations at QOMS. The half-hourly mean BC concentrations are presented in Fig. 4. In the pre-

201 monsoon season, the diurnal BC concentrations remained significantly high from midnight to noon and increased gradually

202 after the lowest value at approximately 15:00. Elevated BC concentrations were also observed in the afternoon during the post-

203 monsoon and winter periods, and high BC concentrations occurred from midnight to noon. The BC concentrations during the

204 monsoon season were significantly lower than those during the other seasons but peaked in the morning and in the afternoon.

205 Previous studies have demonstrated that the local wind system on the northern slope of Mt. Everest is composed of a morning

206 "valley wind", a late morning-afternoon "glacier wind" weakened by "valley wind", and an evening-early night "mountain

207 wind"(Zou et al., 2008). The QOMS is located in the s-shape valley north of Mt. Everest (Ma et al., 2011). The glacier wind

208 and down mountain wind from the south developed in the afternoon and at night, which provided the potential possibility for

209 pollutants from long-distance sources transported to QOMS along the valley and increased the BC concentrations in the non-

210 monsoon periods. The valley wind from the north in the morning could bring the short-distance emissions from cooking or

211 heating in several villages that are located north (approximately 5 km away) of QOMS. The BC concentrations were

212 remarkably low in the monsoon season but peaked in the morning and in the afternoon, which might be due to the local

213 emissions carried by the valley wind from the north.

214 To explain the significant high values from midnight to noon in the pre-monsoon season, the wind direction frequency at

215 QOMS during 0:00-12:00 and 12:00-24:00 are presented in Fig. 5. During the sampling period in the pre-monsoon season, W

216 (west) winds prevailed from midnight to noon (Fig. 5a), accounting for 18.1% of the total wind directions, followed by ENE

217 (east-northeast) winds (16.4%). This is consistent with the discussion above that there are potential impacts on the BC

218 concentrations at QOMS from long-distance human activity emissions, which can be carried by the westerly winds, i.e., down

219 mountain winds (Cong et al., 2015b). Moreover, the WRF-Chem simulation results showed that the profile of equivalent

220 potential temperature (EPT) increased with altitude and the planetary boundary layer height (PBLH) and wind speed were

221 much lower from midnight to noon (Fig. S2), indicating a more stable atmosphere that obstructs the diffusion of BC aerosols.

222 ESE (east-southeast) and NE (northeast) winds prevailed from noon to midnight (Fig. 5b), accounting for 17.6% and 15.3%

223 of the total wind directions, respectively, implying a strengthened glacier wind or mountain wind (from the south), which

224 caused the increase in BC contributed by long-distance sources. During the pre-monsoon season, the strong down-valley wind

225 could transport large amounts of trans-Himalayan pollution from heavily polluted areas of South Asia to QOMS; therefore,

226 the long-distance sources play a major role in the diurnal variation in the BC concentrations at QOMS during this period.

227 **3.2 Comparison of the BC concentrations with other sites on the TP**

228 A previous study has revealed that low BC concentrations in China can be found on the TP, with values of approximately

229 200-1000 ng/m^3 in $PM_{2.1}$ and 300-1500 ng/m^3 in $PM_{9.0}$ (Xin et al., 2015). To better understand the BC loading level, we

230 compared our results with previous studies from other locations over the TP. As shown in Fig. 1, the BC concentrations at

231 Muztagh Ata and Qilian Shan presented low values, which can be regarded as the background concentration level for inland

232 Asia (Cao et al., 2009; Zhao et al., 2012). In contrast, the BC concentration at Lhasa city was higher than that at other sites on

233 the TP, which was mainly contributed by local fossil fuel combustion (Li et al., 2016b). In addition, under the impact of the

234 long-range transport of anthropogenic emissions from the east and significant dust input from the west, the BC concentration

235 at Qinghai Lake also showed a relatively high value (Li et al., 2013). The BC concentration at Beiluhe was slightly higher than

236 that at Qinghai Lake, mainly from the arid regions in northwestern China in spring and from the southern slope of the

237 Himalayas in winter (Wang et al., 2016). Therefore, the long-range transportation from Central Asia and East Asia contributed

238 greatly to the BC aerosols in the northern TP. For the sites in the central and southeastern regions on the TP (e.g., Nam Co and

239 Ranwu), which are isolated from anthropogenic activities with relatively clean atmospheric environments, the BC

240 concentrations at these two sites were above 130 ng/m^3, likely due to the influence of long-range transport from South Asia

241 (Wan et al., 2015; Wang et al., 2016). Compared with the locations on the southern slope of the Himalayas (e.g., NCO-P and

242 Manora Peak), the BC concentration at QOMS was close to that at NCO-P but much lower than that at Manora Peak, which is

243 near the polluted areas in South Asia and largely affected by anthropogenic emissions (Marinoni et al., 2010; Ram et al., 2010).

244 This implies that the combustion emissions from South Asia affect not only the lower latitudes in the vicinity but also the

245 higher latitudes in the Himalayas and the interior of the TP due to long-range transport.

246 **3.3 Potential sources and transport mechanisms of BC in different seasons**

247 The seasonal variation in the BC concentrations was correlated with the combustion intensity of sources and atmospheric

248 circulation. The "Atmospheric Brown Clouds" over South Asia contain large amounts of aerosol components such as the high

249 loading emissions of BC from biomass burning, which can reach the TP within a few days (Ramanathan et al., 2005;

250 Ramanathan and Ramana, 2005; Luthi et al., 2015). A previous study has quantified biomass burning sources contributing to

251 BC aerosols from the Himalayan region of Nepal and India and showed that the major fires were concentrated from March to

252 June; additionally, most fires occurred in the low elevation areas dominated by forests and croplands (Vadrevu et al., 2012).

253 Therefore, we further checked the biomass burning emissions in the Mt. Everest region and its vicinities using the active fire

254 product from the MODIS data during four seasons (August 2015 to April 2016) provided by the FIRMS (Fig. 6). It is clearly

255 shown that there were large numbers of active fire spots in northern and central India, Pakistan and Nepal in winter and in the

256 pre-monsoon season. Moreover, referring to Cong et al. (2015a), the active fire spots represent agricultural combustion and

257 forest fires in this region, which might substantially contribute to BC aerosols. During the monsoon season, insignificant fire

258 spots appeared in South Asia, representing less biomass burning in that period.

259 To further explore the sources and the long-range transport mechanism of BC aerosols at QOMS, we calculated the

260 frequency plots for 5-day backward trajectories arriving 1 km above ground level (Fig. 7). During the non-monsoon seasons,

261 the air masses were affected by the westerly winds. The air masses reaching the Mt. Everest region were mostly from the

262 northwest, indicating that the biomass burning emissions in Pakistan, northern India and Nepal could be transported to the Mt.

263 Everest region. However, for the difference in the combustion intensity, high concentrations of BC were found only during the

264 pre-monsoon season. During the monsoon season, the southerly winds dominated in the Mt. Everest region, and the air masses

265 were mainly from the Arabian Sea and the Bay of Bengal with substantial moisture. At this period, the precipitation on the

266 southern side of the Himalayas was above 1200 mm (Xu et al., 2014), which can improve the wet removal efficiency of BC.

267 Moreover, the biomass combustion emissions in South Asia in this period were very low. Therefore, the BC concentrations at

268 QOMS were close to the background level during the monsoon season. Meanwhile, the local meteorological conditions also

269 play a very important role in the transport of pollutants across the Himalayas from South Asia. Previous studies have shown

270 that the local wind system was mainly composed of up-valley wind on the southern slope and down-valley wind on the northern

271 slope, which facilitates the exchange of air between the bottom and upside of the atmosphere, and facilitates the coupling of

272 air flow between the southern and northern slopes, which allows the pollutants from South Asia to easily cross the Himalayas

273 and be transported to the TP from the valley (Zou et al., 2008; Chen et al., 2012; Cong et al., 2015b; Tripathee et al., 2017;

274 Dhungel et al., 2018).

3.4 Pollution episodes analysis by WRF-Chem modeling

276 In this section, we analyzed four pollution events with BC concentrations above 1000 ng/m^3 in detail, including event A

277 during 8-10 June 2015, event B during 19-22 March 2016, event C during 9-30 April 2016, and event D during 11-14 April

2017. Fig. 8 shows the spatial characteristics of the WRF-Chem modeled surface BC concentrations during the four pollution episodes. It can be seen that the high values of surface BC concentrations always appeared in South Asia, although the high-value centers changed in different pollution events. For event A, the most serious pollution appeared in Nepal and northern India. There was relatively less BC near Mt. Everest in event B than in the other events. However, for event C, the high BC concentration areas were mainly along the southern slope of the Himalayas in Nepal and eastern India, which can highly impact the BC concentrations in the Mt. Everest region. In event D, the high BC concentrations occurred in Nepal and some parts of India. To evaluate the model performance, the temporal variation in measured and simulated BC concentrations at QOMS during these four pollution episodes are displayed in Fig. S3. As shown in Fig. S3, for the four pollution episodes, the WRF-Chem model captured the variation trends of the observed BC concentrations, with correlation coefficients all above 0.8. This implies that the model could reproduce the distribution of BC concentrations in this region. Additionally, comparisons between the modeled wind and precipitation and the wind and precipitation from reanalysis data and in-situ observations indicated that the WRF-Chem model could capture the spatiotemporal variations in the meteorological elements (Fig. S4 and Fig. S5).

The sources and transport mechanisms of BC aerosols during these pollution episodes can be indicated by analyzing the air flow. Fig. 9 shows the variation in the BC concentrations and wind fields at different altitudes in the atmosphere (850 hPa, 500 hPa, and 200 hPa). For event A during the monsoon season, there was a cyclone in northern India at 850 hPa that moved near-surface BC aerosols upward, and then, the southerly winds at 500 hPa and 200 hPa transported the BC aerosols to the Mt. Everest region. For events B-D in the pre-monsoon season, the northwesterly winds prevailed in South Asia at 850 hPa and brought BC from northern India to the southern slope of the Himalayas, and the westerly winds at 500 hPa and 200 hPa transported relatively less BC from northwestern India and Central Asia to the Mt. Everest region. Previous studies also pointed out that BC can be transported across the Himalayas to the Mt. Everest region by the mountain-valley wind system (Zou et al., 2008; Cong et al., 2015b; Dhungel et al., 2018). Thus, we needed to further analyze the impact of the mountain-valley wind on the transportation of BC. Fig. 10 shows the vertical profile of the BC concentration along the QOMS's longitude of 86.95°E. During event A, high concentrations of BC appeared in the upper atmosphere of South Asia, and many BC aerosols were transported to most parts of the TP (Fig. 10a) due to the large-scale transport process. However, for events B-D, high concentrations of BC occurred along the southern slope of the Himalayas, and BC aerosols were only transported to a few areas on the northern slope of the Himalayas such as the Mt. Everest region (Fig. 10b-d) due to the local mountain-valley wind. As shown in Fig. S6, for events B-D, the up-valley wind on the southern side of the Himalayas can move BC aerosols up in the daytime, and the down-valley wind can cause the aerosols to descend in the Mt. Everest region at night.

To sum up, we found that the transport processes of BC aerosols from South Asia to the QOMS were different as the seasons changed. In the monsoon season such as event A, BC aerosols were moved upward by the cyclone in the lower atmosphere and were transported to QOMS by the southerly winds in the upper atmosphere. However, in the pre-monsoon season such as events B-D, the mountain-valley wind played an important role in transporting the BC aerosols from the

310   southern slope of the Himalayas to the Mt. Everest region.

311   **4. Conclusions**

312   In this study, BC concentrations were measured from 15 May 2015 to 31 May 2017 at QOMS on the south edge of the

313   TP. Monthly, daily, and diurnal variations in BC concentrations were calculated to investigate the temporal characteristics and

314   potential sources of BC at QOMS. The results showed that the monthly mean BC concentrations reached the highest value in

315   the pre-monsoon season (923.1 ± 685.8 ng/m^3) and the lowest value in the monsoon season (88.5 ± 29.8 ng/m^3). The average

316   daily BC concentration was equal to 298.8 ± 341.3 ng/m^3, with a maximum in the pre-monsoon season (2772.3 ng/m^3) and a

317   minimum in the monsoon season (36.4 ng/m^3). For the diurnal variation in BC, there was an increase in the afternoon during

318   the non-monsoon periods, and high BC concentrations occurred from midnight to noon, implying that the potential origin of

319   BC was from long-range transport. The BC concentrations remained low but peaked in the morning and in the afternoon during

320   the monsoon period, which might be due to local anthropogenic activities. In addition, the substantially high values of diurnal

321   variation in the BC concentrations in the pre-monsoon season suggest the high contributions of long-distance emissions carried

322   by down-valley wind.

323   The seasonal cycle of BC concentrations at QOMS was closely correlated with the variation in the atmospheric circulation

324   and combustion emissions in South Asia. In the non-monsoon seasons, affected by the westerly winds, the air masses in the

325   Mt. Everest region were largely from Pakistan, northern Indian, and Nepal due to the high loading emissions from vegetation

326   fires. In the monsoon season, the southerly winds prevailed in the Mt. Everest region, and the air masses were mainly from the

327   Arabian Sea and the Bay of Bengal. Under intense precipitation scavenging of BC and extremely low levels of combustion

328   emissions in South Asia, the BC concentrations at QOMS were close to the background level in the monsoon season.

329   For the four heavy pollution episodes that occurred at QOMS with BC concentrations above 1000 ng/m^3, we found that

330   the transport processes of the BC aerosols from South Asia to the Mt. Everest region were different as the seasons changed. In

331   the monsoon season (using the pollution event during 8-10 June 2015 as an example), BC aerosols were efficiently driven

332   upward by the cyclone in the lower atmosphere in South Asia and transported to the Mt. Everest region by the southerly winds

333   in the upper atmosphere. However, during the pre-monsoon season (using the other three pollution events as examples), the

334   mountain-valley wind played an important role in transporting the BC aerosols across the Himalayas to the Mt. Everest region.

335   *Data availability.* All data are available upon requests made to the corresponding author.

336   *Competing interests.* The authors declare that they have no conflict of interest.

337   *Special issue statement.* This article is part of the special issue "Study of ozone, aerosols and radiation over the Tibetan Plateau

338 (SOAR-TP) (ACP/AMT inter-journal SI)". It is not associated with a conference.

345 **References**

346 Anenberg, S. C., Schwartz, J., Shindell, D., Amann, M., Faluvegi, G., Klimont, Z., Janssens-Maenhout, G., Pozzoli, L., Van

347   Dingenen, R., Vignati, E., Emberson, L., Muller, N. Z., West, J. J., Williams, M., Demkine, V., Hicks, W. K., Kuylenstierna,

348   J., Raes, F., and Ramanathan, V.: Global air quality and health co-benefits of mitigating near-term climate change through

349   methane   and   black   carbon   emission   controls,   Environ.   Health   Perspect.,   120,   831-839,

350   https://doi.org/10.1289/ehp.1104301, 2012.

351 Bonasoni, P., Laj, P., Angelini, F., Arduini, J., Bonafe, U., Calzolari, F., Cristofanelli, P., Decesari, S., Facchini, M. C., Fuzzi,

352   S., Gobbi, G. P., Maione, M., Marinoni, A., Petzold, A., Roccato, F., Roger, J. C., Sellegri, K., Sprenger, M., Venzac, H.,

353   Verza, G. P., Villani, P., and Vuillermoz, E.: The ABC-Pyramid Atmospheric Research Observatory in Himalaya for aerosol,

354   ozone and halocarbon measurements, Sci. Total Environ., 391, 252-261, https://doi.org/10.1016/j.scitotenv.2007.10.024,

355   2008.

356 Bond, T. C., Anderson, T. L., and Campbell, D.: Calibration and intercomparison of filter-based measurements of visible light

357   absorption by aerosols, Aerosol Sci. Technol., 30, 582-600, https://doi.org/10.1080/027868299304435, 1999.

358 Bond, T. C.: A technology-based global inventory of black and organic carbon emissions from combustion, J. Geophys. Res.,

359   109, https://doi.org/10.1029/2003jd003697, 2004.

360 Bond, T. C., Doherty, S. J., Fahey, D. W., Forster, P. M., Berntsen, T., DeAngelo, B. J., Flanner, M. G., Ghan, S., Kärcher, B.,

361   Koch, D., Kinne, S., Kondo, Y., Quinn, P. K., Sarofim, M. C., Schultz, M. G., Schulz, M., Venkataraman, C., Zhang, H.,

362   Zhang, S., Bellouin, N., Guttikunda, S. K., Hopke, P. K., Jacobson, M. Z., Kaiser, J. W., Klimont, Z., Lohmann, U., Schwarz,

363   J. P., Shindell, D., Storelvmo, T., Warren, S. G., and Zender, C. S.: Bounding the role of black carbon in the climate system:

364   A scientific assessment, J. Geophys. Res.: Atmos., 118, 5380-5552, https://doi.org/10.1002/jgrd.50171, 2013.

365 Cao, J., Xu, B., He, J., Liu, X., Han, Y., Wang, G., and Zhu, C.: Concentrations, seasonal variations, and transport of

366   carbonaceous aerosols at a remote Mountainous region in western China, Atmos. Environ., 43, 4444-4452,

367   https://doi.org/10.1016/j.atmosenv.2009.06.023, 2009.

368 Chen, X., Su, Z., Ma, Y., and Sun, F.: Analysis of Land-Atmosphere Interactions over the North Region of Mt. Qomolangma

369   (Mt. Everest), Arct. Antarct. Alp. Res., 44, 412-4222012.

370 Chow, J. C., Watson, J. G., Pritchett, L. C., Pierson, W. R., Frazier, C. A., and Purcell, R. G.: The DRI thermal/optical

371   reflectance carbon analysis system: description, evaluation and applications in U.S. air quality studies, Atmos. Environ.,

372   27, 1185-1201, https://doi.org/https://doi.org/10.1016/0960-1686(93)90245-T, 1993.

373 Chow, J. C., Watson, J. G., Crow, D., Lowenthal, D. H., and Merrifield, T.: Comparison of IMPROVE and NIOSH carbon

374   measurements, Aerosol Sci. Technol., 34, 23-34, https://doi.org/10.1080/027868201300081923, 2001.

375 Cong, Z., Kang, S., Kawamura, K., Liu, B., Wan, X., Wang, Z., Gao, S., and Fu, P.: Carbonaceous aerosols on the south edge

13

376   of the Tibetan Plateau: concentrations, seasonality and sources, Atmos. Chem. Phys., 15, 1573-1584,

377   https://doi.org/10.5194/acp-15-1573-2015, 2015a.

378   Cong, Z., Kawamura, K., Kang, S., and Fu, P.: Penetration of biomass-burning emissions from South Asia through the

379   Himalayas: new insights from atmospheric organic acids, Sci. Rep., 5, 9580, https://doi.org/10.1038/srep09580, 2015b.

380   Cooke, W. F., Ramaswamy, V., and Kasibhatla, P.: A general circulation model study of the global carbonaceous aerosol

381   distribution, J. Geophys. Res.: Atmos., 107, ACH 2-1-ACH 2-32, https://doi.org/10.1029/2001JD001274, 2002.

382   Crenn, V., Sciare, J., Croteau, P. L., Verlhac, S., Froehlich, R., Belis, C. A., Aas, W., Aijala, M., Alastuey, A., Artinano, B.,

383   Baisnee, D., Bonnaire, N., Bressi, M., Canagaratna, M., Canonaco, F., Carbone, C., Cavalli, F., Coz, E., Cubison, M. J.,

384   Esser-Gietl, J. K., Green, D. C., Gros, V., Heikkinen, L., Herrmann, H., Lunder, C., Minguillon, M. C., Mocnik, G., O'Dowd,

385   C. D., Ovadnevaite, J., Petit, J. E., Petralia, E., Poulain, L., Priestman, M., Riffault, V., Ripoll, A., Sarda-Esteve, R., Slowik,

386   J. G., Setyan, A., Wiedensohler, A., Baltensperger, U., Prevot, A. S. H., Jayne, J. T., and Favez, O.: ACTRIS ACSM

387   intercomparison - Part 1: Reproducibility of concentration and fragment results from 13 individual Quadrupole Aerosol

388   Chemical Speciation Monitors (Q-ACSM) and consistency with co-located instruments, Atmos. Meas. Tech., 8, 5063-

389   5087, https://doi.org/10.5194/amt-8-5063-2015, 2015.

390   Dhungel, S., Kathayat, B., Mahata, K., and Panday, A.: Transport of regional pollutants through a remote trans-Himalayan

391   valley in Nepal, Atmos. Chem. Phys., 18, 1203-1216, https://doi.org/10.5194/acp-18-1203-2018, 2018.

392   Drinovec, L., Mocnik, G., Zotter, P., Prevot, A. S. H., Ruckstuhl, C., Coz, E., Rupakheti, M., Sciare, J., Mueller, T.,

393   Wiedensohler, A., and Hansen, A. D. A.: The "dual-spot" Aethalometer: an improved measurement of aerosol black carbon

394   with real-time loading compensation, Atmos. Meas. Tech., 8, 1965-1979, https://doi.org/10.5194/amt-8-1965-2015, 2015.

395   Emmons, L. K., Walters, S., Hess, P. G., Lamarque, J. F., Pfister, G. G., Fillmore, D., Granier, C., Guenther, A., Kinnison, D.,

396   Laepple, T., Orlando, J., Tie, X., Tyndall, G., Wiedinmyer, C., Baughcum, S. L., and Kloster, S.: Description and evaluation

397   of the Model for Ozone and Related chemical Tracers, version 4 (MOZART-4), Geosci. Model Dev., 3, 43-67,

398   https://doi.org/10.5194/gmd-3-43-2010, 2010.

399   Fialho, P., Hansen, A. D. A., and Honrath, R. E.: Absorption coefficients by aerosols in remote areas: a new approach to

400   decouple dust and black carbon absorption coefficients using seven-wavelength Aethalometer data, J. Aerosol Sci., 36,

401   267-282, https://doi.org/10.1016/j.jaerosci.2004.09.004, 2005.

402   Flanner, M. G., Zender, C. S., Randerson, J. T., and Rasch, P. J.: Present-day climate forcing and response from black carbon

403   in snow, J. Geophys. Res., 112, https://doi.org/10.1029/2006jd008003, 2007.

404   Gao, X., Shi, Y., Song, R., Giorgi, F., Wang, Y., and Zhang, D.: Reduction of future monsoon precipitation over China:

405   comparison between a high resolution RCM simulation and the driving GCM, Meteorol. Atmos. Phys., 100, 73-86,

406   https://doi.org/10.1007/s00703-008-0296-5, 2008.

407   Grell, G. A., Peckham, S. E., Schmitz, R., McKeen, S. A., Frost, G., Skamarock, W. C., and Eder, B.: Fully coupled "online"

408   chemistry within the WRF model, Atmos. Environ., 39, 6957-6975, https://doi.org/10.1016/j.atmosenv.2005.04.027, 2005.

409   Guenther, A., Karl, T., Harley, P., Wiedinmyer, C., Palmer, P. I., and Geron, C.: Estimates of global terrestrial isoprene

410   emissions using MEGAN (Model of Emissions of Gases and Aerosols from Nature), Atmos. Chem. Phys., 6, 3181-3210,

411   https://doi.org/10.5194/acp-6-3181-2006, 2006.

412   Hansen, A. D. A., Rosen, H., and Novakov, T.: The aethalometer — An instrument for the real-time measurement of optical

413   absorption by aerosol particles, Sci. Total Environ., 36, 191-196, https://doi.org/10.1016/0048-9697(84)90265-1, 1984.

414   Hansen, J., Sato, M., Ruedy, R., Lacis, A., and Oinas, V.: Global warming in the twenty-first century: An alternative scenario,

415   Proc. Natl. Acad. Sci. U. S. A., 97, 9875-9880, https://doi.org/10.1073/pnas.170278997, 2000.

416   He, C., Li, Q., Liou, K. N., Takano, Y., Gu, Y., Qi, L., Mao, Y., and Leung, L. R.: Black carbon radiative forcing over the

417   Tibetan Plateau, Geophys. Res. Lett., 41, 7806-7813, https://doi.org/doi:10.1002/2014GL062191, 2014a.

418   He, C., Li, Q., Liou, K. N., Zhang, J., Qi, L., Mao, Y., Gao, M., Lu, Z., Streets, D. G., Zhang, Q., Sarin, M. M., and Ram, K.:

419   A global 3-D CTM evaluation of black carbon in the Tibetan Plateau, Atmos. Chem. Phys., 14, 7091-7112,

420   https://doi.org/10.5194/acp-14-7091-2014, 2014b.

421   He, C., Takano, Y., Liou, K.-N., Yang, P., Li, Q., and Chen, F.: Impact of Snow Grain Shape and Black Carbon–Snow Internal

422   Mixing on Snow Optical Properties: Parameterizations for Climate Models, J. Clim., 30, 10019-10036,

423   https://doi.org/10.1175/jcli-d-17-0300.1, 2017.

424   Hyvarinen, A. P., Vakkari, V., Laakso, L., Hooda, R. K., Sharma, V. P., Panwar, T. S., Beukes, J. P., van Zyl, P. G., Josipovic,

425   M., Garland, R. M., Andreae, M. O., Poeschl, U., and Petzold, A.: Correction for a measurement artifact of the Multi-

426   Angle Absorption Photometer (MAAP) at high black carbon mass concentration levels, Atmos. Meas. Tech., 6, 81-90,

427   https://doi.org/10.5194/amt-6-81-2013, 2013.

428   Jacobson, M. Z.: Strong radiative heating due to the mixing state of black carbon in atmospheric aerosols, Nature, 409, 695-

429   697, https://doi.org/10.1038/35055518, 2001.

430   Jacobson, M. Z.: Control of fossil-fuel particulate black carbon and organic matter, possibly the most effective method of

431   slowing global warming, J. Geophys. Res., 107, https://doi.org/10.1029/2001JD001376, 2002.

432   Ji, Z., Kang, S., Cong, Z., Zhang, Q., and Yao, T.: Simulation of carbonaceous aerosols over the Third Pole and adjacent

433   regions: distribution, transportation, deposition, and climatic effects, Clim. Dyn., 45, 2831-2846,

434   https://doi.org/10.1007/s00382-015-2509-1, 2015.

435   Ji, Z.: Modeling black carbon and its potential radiative effects over the Tibetan Plateau, Adv. Clim. Change. Res., 7, 139-144,

436   https://doi.org/10.1016/j.accre.2016.10.002, 2016.

437   Jurado, E., Dachs, J., Duarte, C. M., and Simó, R.: Atmospheric deposition of organic and black carbon to the global oceans,

438   Atmos. Environ., 42, 7931-7939, https://doi.org/10.1016/j.atmosenv.2008.07.029, 2008.

439   Kang, S., Xu, Y., You, Q., Fluegel, W.-A., Pepin, N., and Yao, T.: Review of climate and cryospheric change in the Tibetan

440   Plateau, Environ. Res. Lett., 5, 015101, https://doi.org/10.1088/1748-9326/5/1/015101, 2010.

441 Kang, S., Chen, P., Li, C., Liu, B., and Cong, Z.: Atmospheric Aerosol Elements over the Inland Tibetan Plateau: Concentration,

442   Seasonality, and Transport, Aerosol Air Qual. Res., 16, 789-800, https://doi.org/10.4209/aaqr.2015.05.0307, 2016.

443 Kopacz, M., Mauzerall, D. L., Wang, J., Leibensperger, E. M., Henze, D. K., and Singh, K.: Origin and radiative forcing of

444   black carbon transported to the Himalayas and Tibetan Plateau, Atmos. Chem. Phys., 11, 2837-2852,

445   https://doi.org/10.5194/acp-11-2837-2011, 2011.

446 Laborde, M., Schnaiter, M., Linke, C., Saathoff, H., Naumann, K. H., Mohler, O., Berlenz, S., Wagner, U., Taylor, J. W., Liu,

447   D., Flynn, M., Allan, J. D., Coe, H., Heimerl, K., Dahlkotter, F., Weinzierl, B., Wollny, A. G., Zanatta, M., Cozic, J., Laj,

448   P., Hitzenberger, R., Schwarz, J. P., and Gysel, M.: Single Particle Soot Photometer intercomparison at the AIDA chamber,

449   Atmos. Meas. Tech., 5, 3077-3097, https://doi.org/10.5194/amt-5-3077-2012, 2012.

450 Lee, W. L., Liou, K. N., He, C. L., Liang, H. C., Wang, T. C., Li, Q. B., Liu, Z. X., and Yue, Q.: Impact of absorbing aerosol

451   deposition on snow albedo reduction over the southern Tibetan plateau based on satellite observations, Theor. Appl.

452   Climatol., 129, 1373-1382, https://doi.org/10.1007/s00704-016-1860-4, 2017.

453 Li, C., Bosch, C., Kang, S., Andersson, A., Chen, P., Zhang, Q., Cong, Z., Chen, B., Qin, D., and Gustafsson, O.: Sources of

454   black carbon to the Himalayan-Tibetan Plateau glaciers, Nat. Commun., 7, 12574, https://doi.org/10.1038/ncomms12574,

455   2016a.

456 Li, C., Chen, P., Kang, S., Yan, F., Hu, Z., Qu, B., and Sillanpää, M.: Concentrations and light absorption characteristics of

457   carbonaceous aerosol in PM 2.5 and PM 10 of Lhasa city, the Tibetan Plateau, Atmos. Environ., 127, 340-346,

458   https://doi.org/10.1016/j.atmosenv.2015.12.059, 2016b.

459 Li, C., Yan, F., Kang, S., Chen, P., Han, X., Hu, Z., Zhang, G., Hong, Y., Gao, S., Qu, B., Zhu, Z., Li, J., Chen, B., and Sillanpää,

460   M.: Re-evaluating black carbon in the Himalayas and the Tibetan Plateau: concentrations and deposition, Atmos. Chem.

461   Phys., 17, 11899-11912, https://doi.org/10.5194/acp-17-11899-2017, 2017a.

462 Li, J., Wang, G., Wang, X., Cao, J., Sun, T., Cheng, C., Meng, J., Hu, T., and Liu, S.: Abundance, composition and source of

463   atmospheric PM2.5 at a remote site in the Tibetan Plateau, China, Tellus B, 65, 20281,

464   https://doi.org/10.3402/tellusb.v65i0.20281, 2013.

465 Li, X., Kang, S., He, X., Qu, B., Tripathee, L., Jing, Z., Paudyal, R., Li, Y., Zhang, Y., Yan, F., Li, G., and Li, C.: Light-

466   absorbing impurities accelerate glacier melt in the Central Tibetan Plateau, Sci. Total Environ., 587, 482-490,

467   https://doi.org/10.1016/j.scitotenv.2017.02.169, 2017b.

468 Li, X., Kang, S., Zhang, G., Qu, B., Tripathee, L., Paudyal, R., Jing, Z., Zhang, Y., Yan, F., Li, G., Cui, X., Xu, R., Hu, Z., and

469   Li, C.: Light-absorbing impurities in a southern Tibetan Plateau glacier: Variations and potential impact on snow albedo

470   and radiative forcing, Atmos. Res., 200, 77-87, https://doi.org/10.1016/j.atmosres.2017.10.002, 2018.

471 Lu, A., Kang, S., Li, Z., and Theakstone, W. H.: Altitude effects of climatic variation on Tibetan Plateau and its vicinities, J.

Earth Sci., 21, 189-198, https://doi.org/10.1007/s12583-010-0017-0, 2010.

Lu, Z., Streets, D. G., Zhang, Q., and Wang, S.: A novel back-trajectory analysis of the origin of black carbon transported to the Himalayas and Tibetan Plateau during 1996-2010, Geophys. Res. Lett., 39, L01809, https://doi.org/10.1029/2011gl049903, 2012.

Luthi, Z. L., Skerlak, B., Kim, S. W., Lauer, A., Mues, A., Rupakheti, M., and Kang, S.: Atmospheric brown clouds reach the Tibetan Plateau by crossing the Himalayas, Atmos. Chem. Phys., 15, 6007-6021, https://doi.org/10.5194/acp-15-6007-2015, 2015.

Ma, Y., Wang, Y., Zhong, L., Wu, R., Wang, S., and Li, M.: The Characteristics of Atmospheric Turbulence and Radiation Energy Transfer and the Structure of Atmospheric Boundary Layer over the Northern Slope Area of Himalaya, J. Meteorol. Soc. Jpn., 89A, 345-353, https://doi.org/10.2151/jmsj.2011-A24, 2011.

Marinoni, A., Cristofanelli, P., Laj, P., Duchi, R., Calzolari, F., Decesari, S., Sellegri, K., Vuillermoz, E., Verza, G. P., Villani, P., and Bonasoni, P.: Aerosol mass and black carbon concentrations, a two year record at NCO-P (5079 m, Southern Himalayas), Atmos. Chem. Phys., 10, 8551-8562, https://doi.org/10.5194/acp-10-8551-2010, 2010.

Menon, S., Koch, D., Beig, G., Sahu, S., Fasullo, J., and Orlikowski, D.: Black carbon aerosols and the third polar ice cap, Atmos. Chem. Phys., 10, 4559-4571, https://doi.org/10.5194/acp-10-4559-2010, 2010.

Ming, J., Cachier, H., Xiao, C., Qin, D., Kang, S., Hou, S., and Xu, J.: Black carbon record based on a shallow Himalayan ice core and its climatic implications, Atmos. Chem. Phys., 8, 1343-1352, https://doi.org/10.5194/acp-8-1343-2008, 2008.

Oshima, N., Kondo, Y., Moteki, N., Takegawa, N., Koike, M., Kita, K., Matsui, H., Kajino, M., Nakamura, H., Jung, J. S., and Kim, Y. J.: Wet removal of black carbon in Asian outflow: Aerosol Radiative Forcing in East Asia (A-FORCE) aircraft campaign, J. Geophys. Res., 117, D03204, https://doi.org/10.1029/2011jd016552, 2012.

Park, S. S., Hansen, A. D. A., and Cho, S. Y.: Measurement of real time black carbon for investigating spot loading effects of Aethalometer data, Atmos. Environ., 44, 1449-1455, https://doi.org/10.1016/j.atmosenv.2010.01.025, 2010.

Petzold, A., and Schonlinner, M.: Multi-angle absorption photometry - a new method for the measurement of aerosol light absorption and atmospheric black carbon, J. Aerosol Sci., 35, 421-441, https://doi.org/10.1016/j.jaerosci.2003.09.005, 2004.

Praveen, P. S., Ahmed, T., Kar, A., Rehman, I. H., and Ramanathan, V.: Link between local scale BC emissions and large scale atmospheric solar absorption, Atmos. Chem. Phys., 12, 1173-1187, https://doi.org/10.5194/acp-12-1173-2012, 2012.

Qu, B., Ming, J., Kang, S.-C., Zhang, G.-S., Li, Y.-W., Li, C.-D., Zhao, S.-Y., Ji, Z.-M., and Cao, J.-J.: The decreasing albedo of Zhadang glacier on western Nyainqentanglha and the role of light-absorbing impurities, Atmos. Chem. Phys., 14, 11117-11128, https://doi.org/10.5194/acp-14-11117-2014, 2014.

Rajesh, T. A., and Ramachandran, S.: Black carbon aerosol mass concentration, absorption and single scattering albedo from single and dual spot aethalometers: Radiative implications, J. Aerosol Sci., 119, 77-90,

504   https://doi.org/10.1016/j.jaerosci.2018.02.001, 2018.

505   Ram, K., Sarin, M. M., and Hegde, P.: Long-term record of aerosol optical properties and chemical composition from a high-

506   altitude site (Manora Peak) in Central Himalaya, Atmos. Chem. Phys., 10, 11791-11803, https://doi.org/10.5194/acp-10-

507   11791-2010, 2010.

508   Ramanathan, V., Chung, C., Kim, D., Bettge, T., Buja, L., Kiehl, J. T., Washington, W. M., Fu, Q., Sikka, D. R., and Wild, M.:

509   Atmospheric brown clouds: impacts on South Asian climate and hydrological cycle, P. Natl. Acad. Sci. USA, 102, 5326-

510   5333, https://doi.org/10.1073/pnas.0500656102, 2005.

511   Ramanathan, V., and Ramana, M. V.: Persistent, Widespread, and Strongly Absorbing Haze Over the Himalayan Foothills and

512   the Indo-Gangetic Plains, Pure appl. geophys., 162, 1609-1626, https://doi.org/10.1007/s00024-005-2685-8, 2005.

513   Ramanathan, V., and Carmichael, G.: Global and Regional Climate Changes Due to Black Carbon, Nature Geosci., 1, 221-227,

514   https://doi.org/10.1038/ngeo156, 2008.

515   Sandradewi, J., Prevot, A., Szidat, S., Perron, N., Alfarra, M., A Lanz, V., Weingartner, E., and Baltensperger, U.: Using aerosol

516   light absorption measurements for the quantitative determination of wood burning and traffic emission contributions to

517   particulate matter, Environ. Sci. Technol., 42, 3316-3323, https://doi.org/10.1021/es702253m, 2008a.

518   Sandradewi, J., Prevot, A., Weingartner, E., Schmidhauser, R., Gysel, M., and Baltensperger, U.: A study of wood burning and

519   traffic aerosols in an Alpine valley using a multi-wavelength Aethalometer, Atmos. Environ., 42, 101-112,

520   https://doi.org/10.1016/j.atmosenv.2007.09.034, 2008b.

521   Schauer, J. J., Mader, B. T., Deminter, J. T., Heidemann, G., Bae, M. S., Seinfeld, J. H., Flagan, R. C., Cary, R. A., Smith, D.,

522   Huebert, B. J., Bertram, T., Howell, S., Kline, J. T., Quinn, P., Bates, T., Turpin, B., Lim, H. J., Yu, J. Z., Yang, H., and

523   Keywood, M. D.: ACE-Asia intercomparison of a thermal-optical method for the determination of particle-phase organic

524   and elemental carbon, Environ. Sci. Technol., 37, 993-1001, https://doi.org/10.1021/es020622f, 2003.

525   Schwarz, J. P., Spackman, J. R., Gao, R. S., Perring, A. E., Cross, E., Onasch, T. B., Ahern, A., Wrobel, W., Davidovits, P.,

526   Olfert, J., Dubey, M. K., Mazzoleni, C., and Fahey, D. W.: The Detection Efficiency of the Single Particle Soot Photometer,

527   Aerosol Sci. Technol., 44, 612-628, https://doi.org/10.1080/02786826.2010.481298, 2010.

528   Skamarock, W. C., Klemp, J. B., Dudhia, J., Gill, D. O., Barker, D. M., Wang, W., and Powers, J. G.: A Description of the

529   Advanced Research WRF Version 2, NCAR Technical Note NCAR/TN-468+STR, https://doi.org/doi:10.5065/D6DZ069T,

530   2005.

531   Stein, A. F., Draxler, R. R., Rolph, G. D., Stunder, B. J. B., Cohen, M. D., and Ngan, F.: NOAA'S HYSPLIT ATMOSPHERIC

532   TRANSPORT AND DISPERSION MODELING SYSTEM, Bull. Am. Meteorol. Soc., 96, 2059-2077,

533   https://doi.org/10.1175/bams-d-14-00110.1, 2015.

534   Stephens, M., Turner, N., and Sandberg, J.: Particle identification by laser-induced incandescence in a solid-state laser cavity,

535   Appl. Opt., 42, 3726-3736, https://doi.org/10.1364/ao.42.003726, 2003.

536   Tripathee, L., Kang, S., Rupakheti, D., Cong, Z., Zhang, Q., and Huang, J.: Chemical characteristics of soluble aerosols over

537   the central Himalayas: insights into spatiotemporal variations and sources, Environ. Sci. Pollut. Res., 24, 24454-24472,

538   https://doi.org/10.1007/s11356-017-0077-0, 2017.

539   Vadrevu, K. P., Ellicott, E., Giglio, L., Badarinath, K. V. S., Vermote, E., Justice, C., and Lau, W. K. M.: Vegetation fires in the

540   himalayan region – Aerosol load, black carbon emissions and smoke plume heights, Atmos. Environ., 47, 241-251,

541   https://doi.org/10.1016/j.atmosenv.2011.11.009, 2012.

542   Virkkula, A., Makela, T., Hillamo, R., Yli-Tuomi, T., Hirsikko, A., Hameri, K., and Koponen, I. K.: A simple procedure for

543   correcting loading effects of aethalometer data, J. Air Waste Manage. Assoc., 57, 1214-1222, https://doi.org/10.3155/1047-

544   3289.57.10.1214, 2007.

545   Wan, X., Kang, S., Wang, Y., Xin, J., Liu, B., Guo, Y., Wen, T., Zhang, G., and Cong, Z.: Size distribution of carbonaceous

546   aerosols at a high-altitude site on the central Tibetan Plateau (Nam Co Station, 4730ma.s.l.), Atmos. Res., 153, 155-164,

547   https://doi.org/10.1016/j.atmosres.2014.08.008, 2015.

548   Wang, M., Xu, B., Wang, N., Cao, J., Tie, X., Wang, H., Zhu, C., and Yang, W.: Two distinct patterns of seasonal variation of

549   airborne   black   carbon   over   Tibetan   Plateau,   Sci.   Total   Environ.,   573,   1041-1052,

550   https://doi.org/10.1016/j.scitotenv.2016.08.184, 2016.

551   Wiedinmyer, C., Akagi, S. K., Yokelson, R. J., Emmons, L. K., Al-Saadi, J. A., Orlando, J. J., and Soja, A. J.: The Fire

552   INventory from NCAR (FINN): a high resolution global model to estimate the emissions from open burning, Geosci.

553   Model Dev., 4, 625-641, https://doi.org/10.5194/gmd-4-625-2011, 2011.

554   Wu, G., Xu, B., Zhang, C., and Gao, S.: Atmospheric dust aerosols over the Eastern Pamirs: major element concentrations and

555   composition, Environ. Earth Sci., 61, 1227-1237, https://doi.org/10.1007/s12665-009-0446-1, 2010.

556   Xin, J. Y., Wang, Y. S., Pan, Y. P., Ji, D. S., Liu, Z. R., Wen, T. X., Wang, Y. H., Li, X. R., Sun, Y., Sun, J., Wang, P. C., Wang,

557   G. H., Wang, X. M., Cong, Z. Y., Song, T., Hu, B., Wang, L. L., Tang, G. Q., Gao, W. K., Guo, Y. H., Miao, H. Y., Tian, S.

558   L., and Wang, L.: The Campaign on Atmospheric Aerosol Research Network of China: CARE-China, Bull. Am. Meteorol.

559   Soc., 96, 1137-1155, https://doi.org/10.1175/bams-d-14-00039.1, 2015.

560   Xu, B., Wang, M., Joswiak, D. R., Cao, J., Yao, T., Wu, G., Yang, W., and Zhao, H.: Deposition of anthropogenic aerosols in

561   a southeastern Tibetan glacier, J. Geophys. Res., 114, D17209, https://doi.org/10.1029/2008JD011510, 2009.

562   Xu, C., Ma, Y. M., Panday, A., Cong, Z. Y., Yang, K., Zhu, Z. K., Wang, J. M., Amatya, P. M., and Zhao, L.: Similarities and

563   differences of aerosol optical properties between southern and northern sides of the Himalayas, Atmos. Chem. Phys., 14,

564   3133-3149, https://doi.org/10.5194/acp-14-3133-2014, 2014.

565   Xu, Y., Ramanathan, V., and Washington, W. M.: Observed high-altitude warming and snow cover retreat over Tibet and the

566   Himalayas enhanced by black carbon aerosols, Atmos. Chem. Phys., 16, 1303-1315, https://doi.org/10.5194/acp-16-1303-

567   2016, 2016.

568 Yang, J., Duan, K., Kang, S., Shi, P., and Ji, Z.: Potential feedback between aerosols and meteorological conditions in a heavy

569   pollution event over the Tibetan Plateau and Indo-Gangetic Plain, Clim. Dyn., 48, 2901-2917,

570   https://doi.org/10.1007/s00382-016-3240-2, 2017.

571 Yang, J., Kang, S., Ji, Z., and Chen, D.: Modeling the Origin of Anthropogenic Black Carbon and Its Climatic Effect Over the

572   Tibetan Plateau and Surrounding Regions, J. Geophys. Res.: Atmos., n/a-n/a, https://doi.org/10.1002/2017JD027282, 2018.

573 Yang, M., Howell, S. G., Zhuang, J., and Huebert, B. J.: Attribution of aerosol light absorption to black carbon, brown carbon,

574   and dust in China - interpretations of atmospheric measurements during EAST-AIRE, Atmos. Chem. Phys., 9, 2035-2050,

575   https://doi.org/10.5194/acp-9-2035-2009, 2009.

576 Yang, S., Xu, B., Cao, J., Zender, C. S., and Wang, M.: Climate effect of black carbon aerosol in a Tibetan Plateau glacier,

577   Atmos. Environ., 111, 71-78, https://doi.org/10.1016/j.atmosenv.2015.03.016, 2015.

578 Yao, T., Thompson, L. G., Mosbrugger, V., Zhang, F., Ma, Y., Luo, T., Xu, B., Yang, X., Joswiak, D. R., Wang, W., Joswiak,

579   M. E., Devkota, L. P., Tayal, S., Jilani, R., and Fayziev, R.: Third Pole Environment (TPE), Environ. Dev., 3, 52-64,

580   https://doi.org/10.1016/j.envdev.2012.04.002, 2012.

581 Zhang, Q., Streets, D. G., Carmichael, G. R., He, K. B., Huo, H., Kannari, A., Klimont, Z., Park, I. S., Reddy, S., Fu, J. S.,

582   Chen, D., Duan, L., Lei, Y., Wang, L. T., and Yao, Z. L.: Asian emissions in 2006 for the NASA INTEX-B mission, Atmos.

583   Chem. Phys., 9, 5131-5153, https://doi.org/10.5194/acp-9-5131-2009, 2009.

584 Zhang, R., Wang, H., Qian, Y., Rasch, P. J., Easter, R. C., Ma, P. L., Singh, B., Huang, J., and Fu, Q.: Quantifying sources,

585   transport, deposition, and radiative forcing of black carbon over the Himalayas and Tibetan Plateau, Atmos. Chem. Phys.,

586   15, 6205-6223, https://doi.org/10.5194/acp-15-6205-2015, 2015.

587 Zhang, X., Ming, J., Li, Z., Wang, F., and Zhang, G.: The online measured black carbon aerosol and source orientations in the

588   Nam Co region, Tibet, Environ. Sci. Pollut. Res., 24, 25021-25033, https://doi.org/10.1007/s11356-017-0165-1, 2017a.
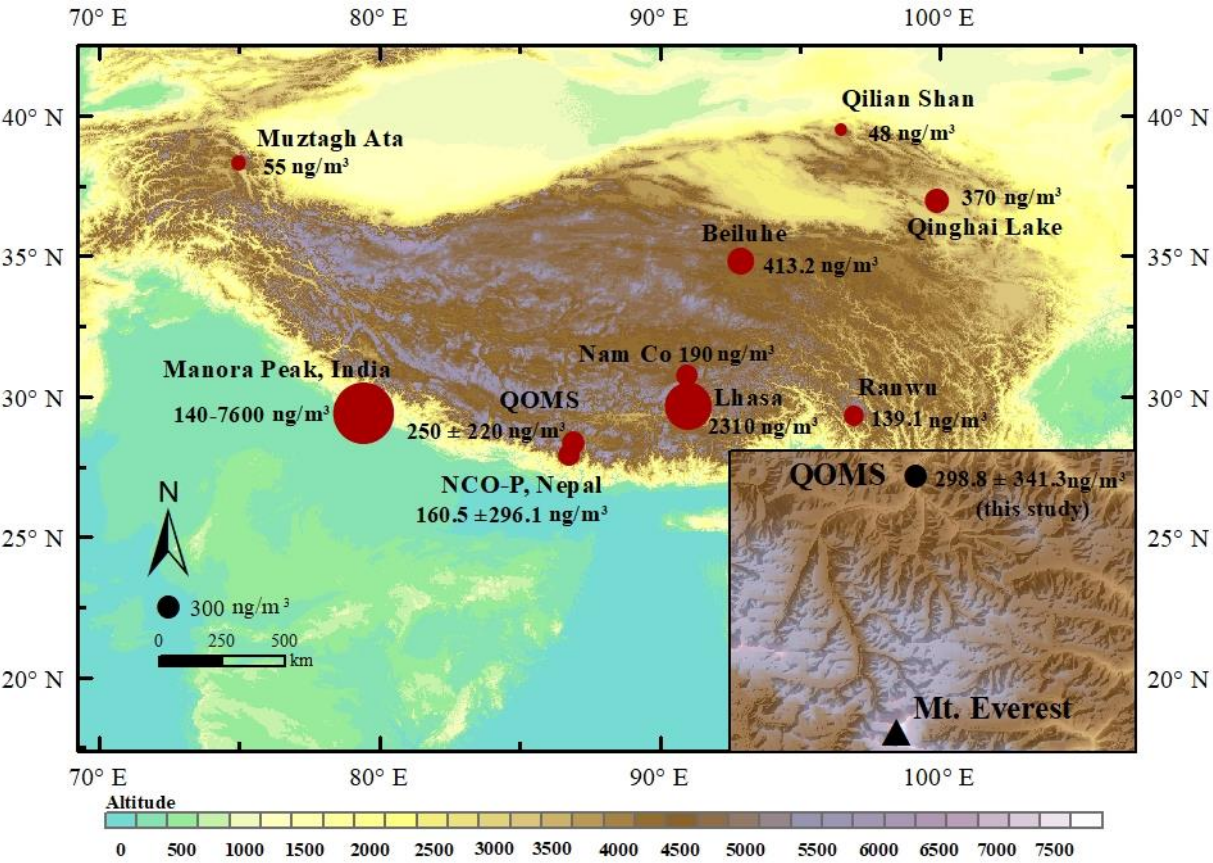
589 Zhang, Y., Kang, S., Cong, Z., Schmale, J., Sprenger, M., Li, C., Yang, W., Gao, T., Sillanpää, M., Li, X., Liu, Y., Chen, P., and

590   Zhang, X.: Light-absorbing impurities enhance glacier albedo reduction in the southeastern Tibetan plateau, J. Geophys.

591   Res.: Atmos., 122, 6915-6933, https://doi.org/10.1002/2016JD026397, 2017b.

592 Zhao, S., Ming, J., Xiao, C., Sun, W., and Qin, X.: A preliminary study on measurements of black carbon in the atmosphere of

593   northwest Qilian Shan, J. Environ. Sci., 24, 152-159, https://doi.org/10.1016/s1001-0742(11)60739-0, 2012.

594 Zhu, C.-S., Cao, J.-J., Hu, T.-F., Shen, Z.-X., Tie, X.-X., Huang, H., Wang, Q.-Y., Huang, R.-J., Zhao, Z.-Z., Mocnik, G., and

595   Hansen, A. D. A.: Spectral dependence of aerosol light absorption at an urban and a remote site over the Tibetan Plateau,

596   Sci. Total Environ., 590, 14-21, https://doi.org/10.1016/j.scitotenv.2017.03.057, 2017.

597 Zou, H., Zhou, L., Ma, S., Li, P., Wang, W., Li, A., Jia, J., and Gao, D.: Local wind system in the Rongbuk Valley on the

598   northern slope of Mt. Everest, Geophys. Res. Lett., 35, L13813, https://doi.org/10.1029/2008gl033466, 2008.
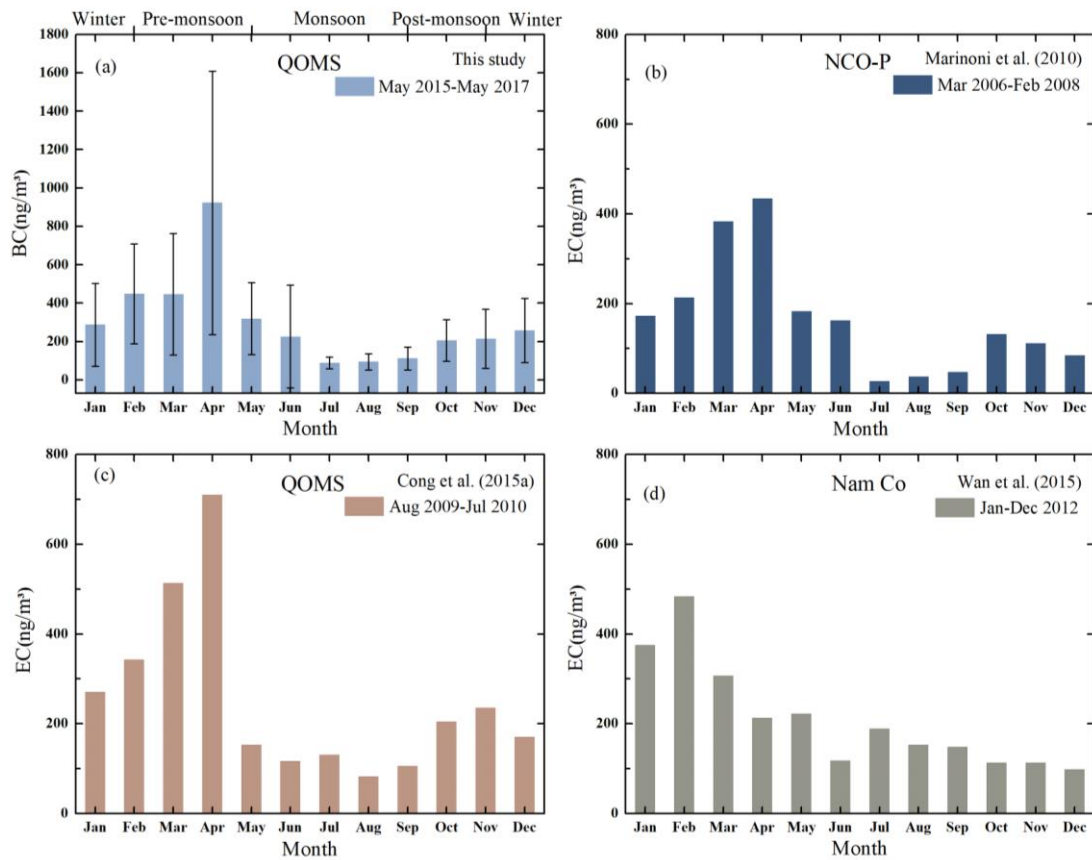
599

600

607

Figure 2. (a) Monthly mean BC concentrations at QOMS from May 2015 to May 2017 in this study; (b) Monthly mean EC at NCO-P from March 2006 to February 2008 from Marinoni et al. (2010); (c) Monthly mean EC at QOMS from August 2009 to July 2010 from Cong et al. (2015a); (d) Monthly mean EC at Nam Co station from January to December during 2012 from Wan et al. (2015).
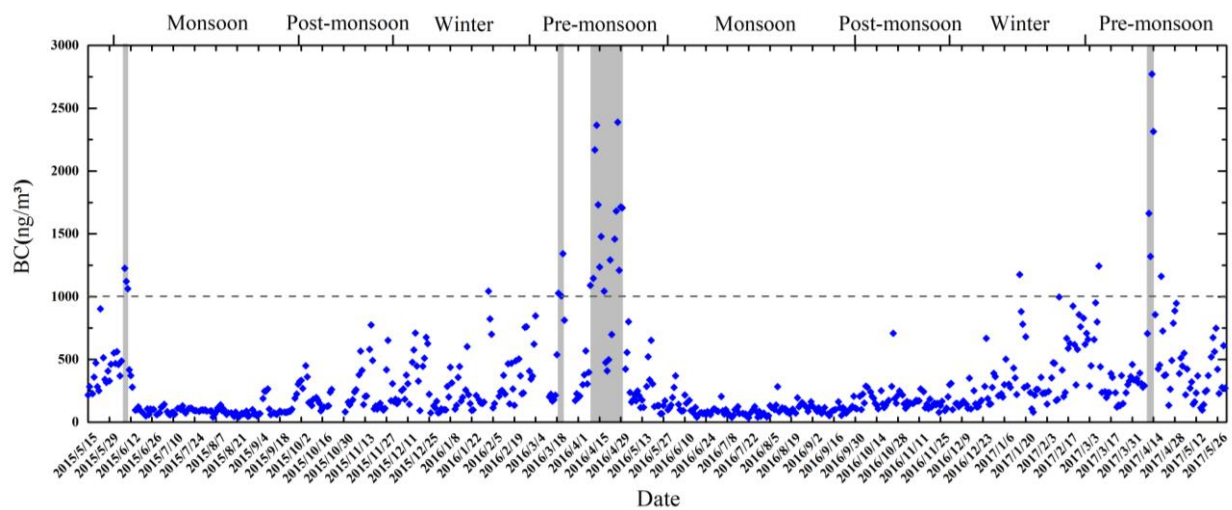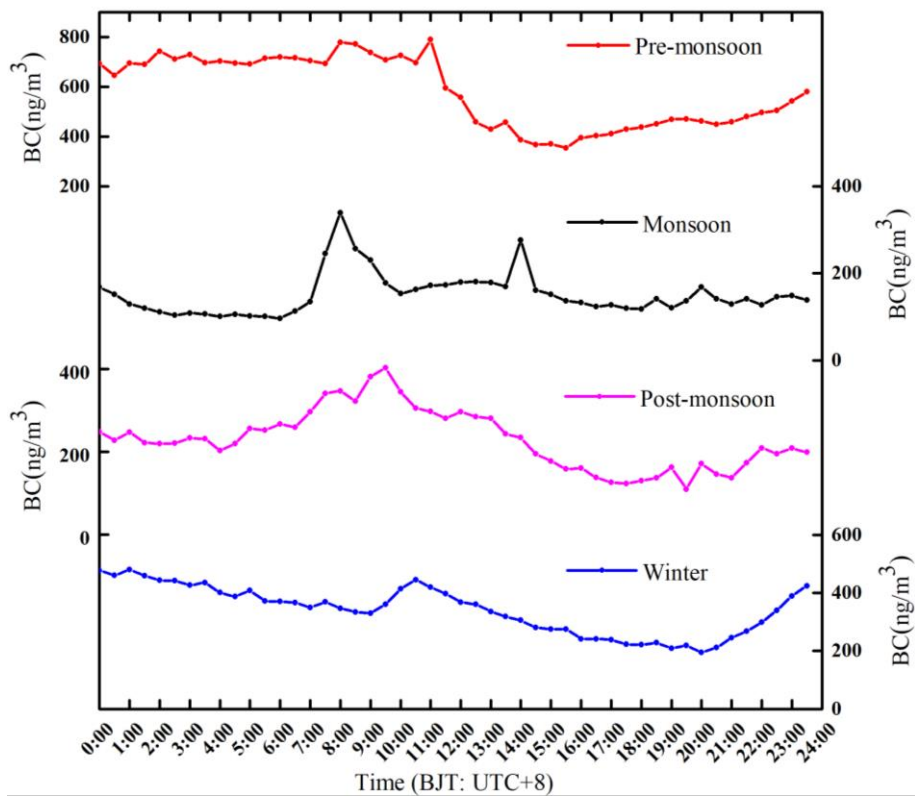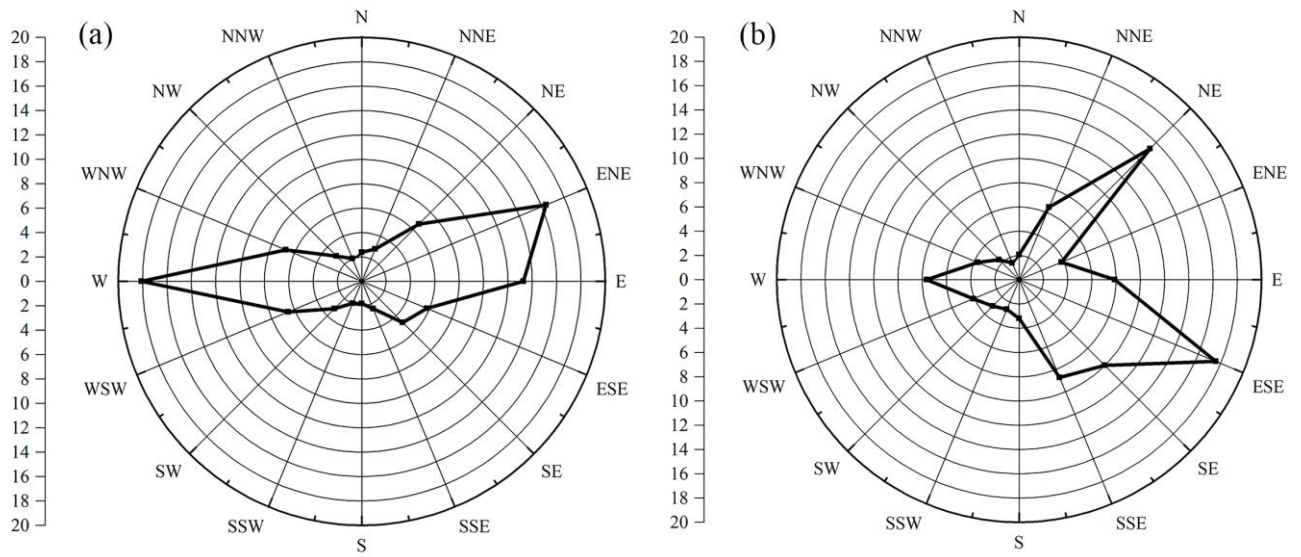
611

Figure 3. Daily mean BC concentrations at QOMS during study period (the gray bars represent the continuous high values more than 1000 ng/m³).

616

Figure 4. Diurnal variation in BC concentrations (every half an hour) at QOMS during study period.

618

619

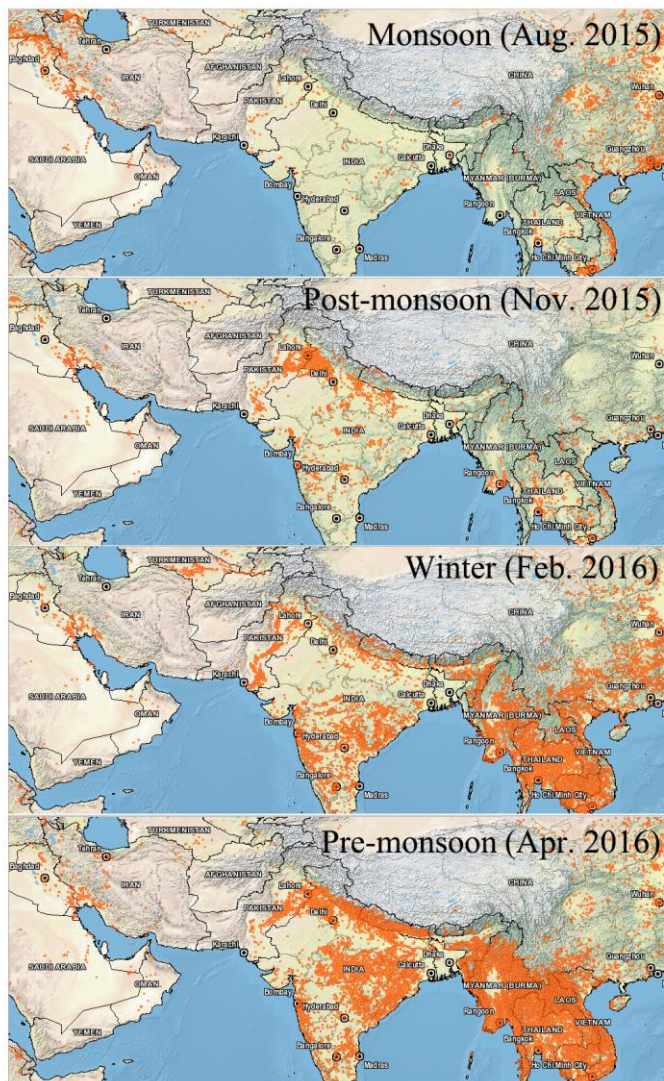**Figure 5.** Wind direction frequency at QOMS in the pre-monsoon season (a) 0:00-12:00; (b) 12:00-24:00.

621

622

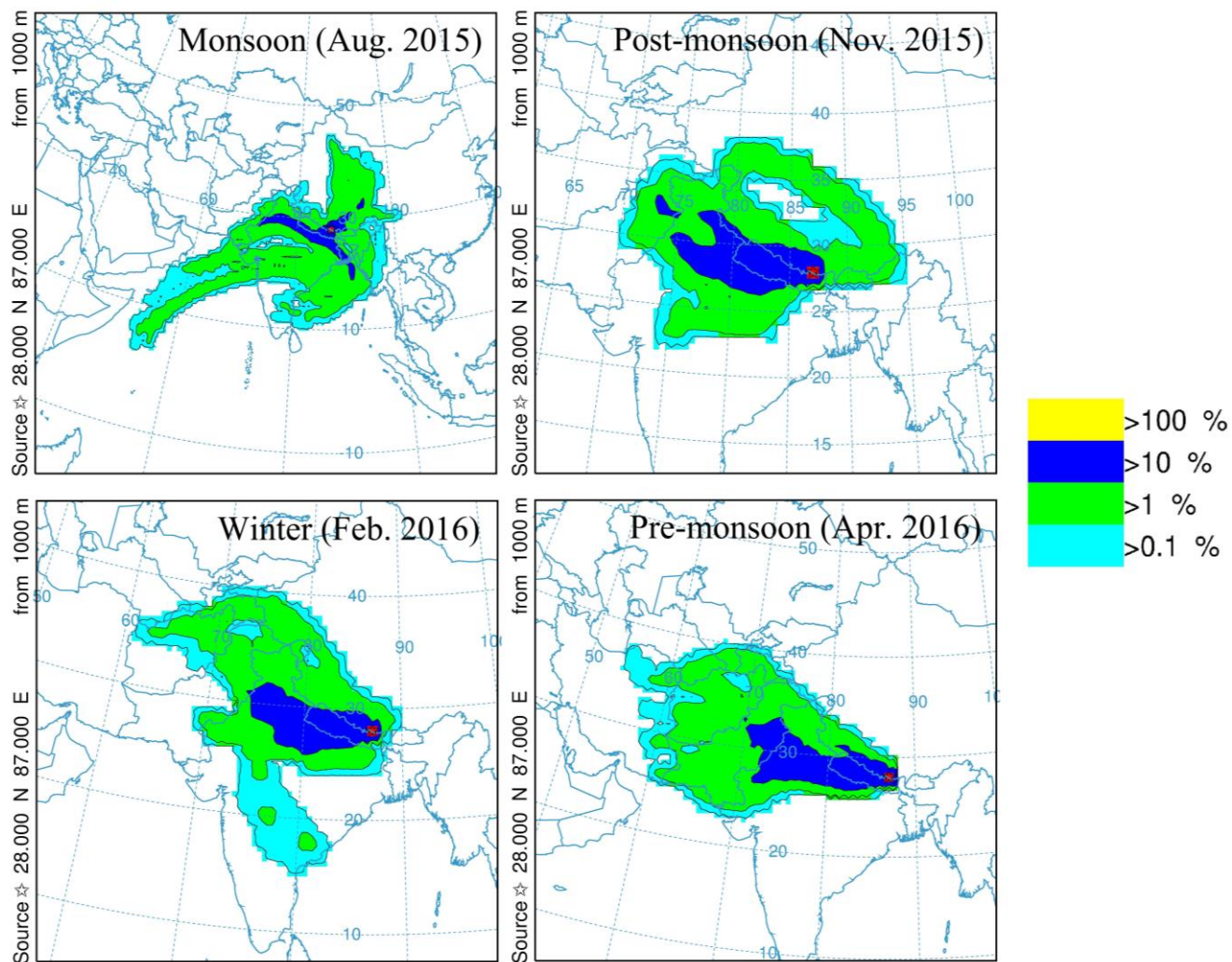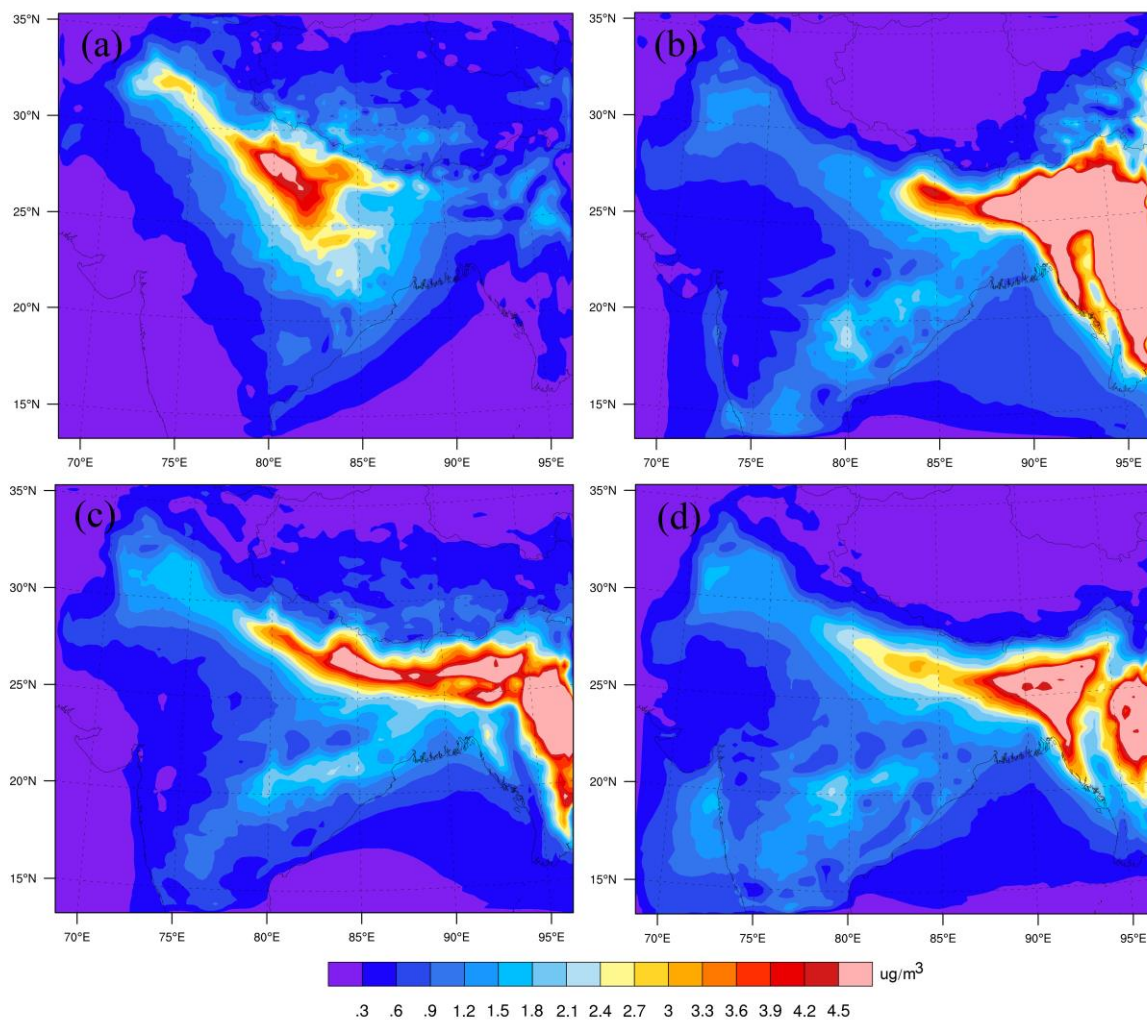**Figure 6.** Distribution of fire spots in different seasons from August 2015 to April 2016.

624

625

Figure 7. Frequency plots for 5-day backward trajectories calculated by HYSPLIT model at QOMS in different seasons from August
2015 to April 2016.

628

629

Figure 8. Mean BC concentration simulated by WRF-Chem model at QOMS and its vicinities: (a) event A; (b) event B; (c) event C; (d) event D.
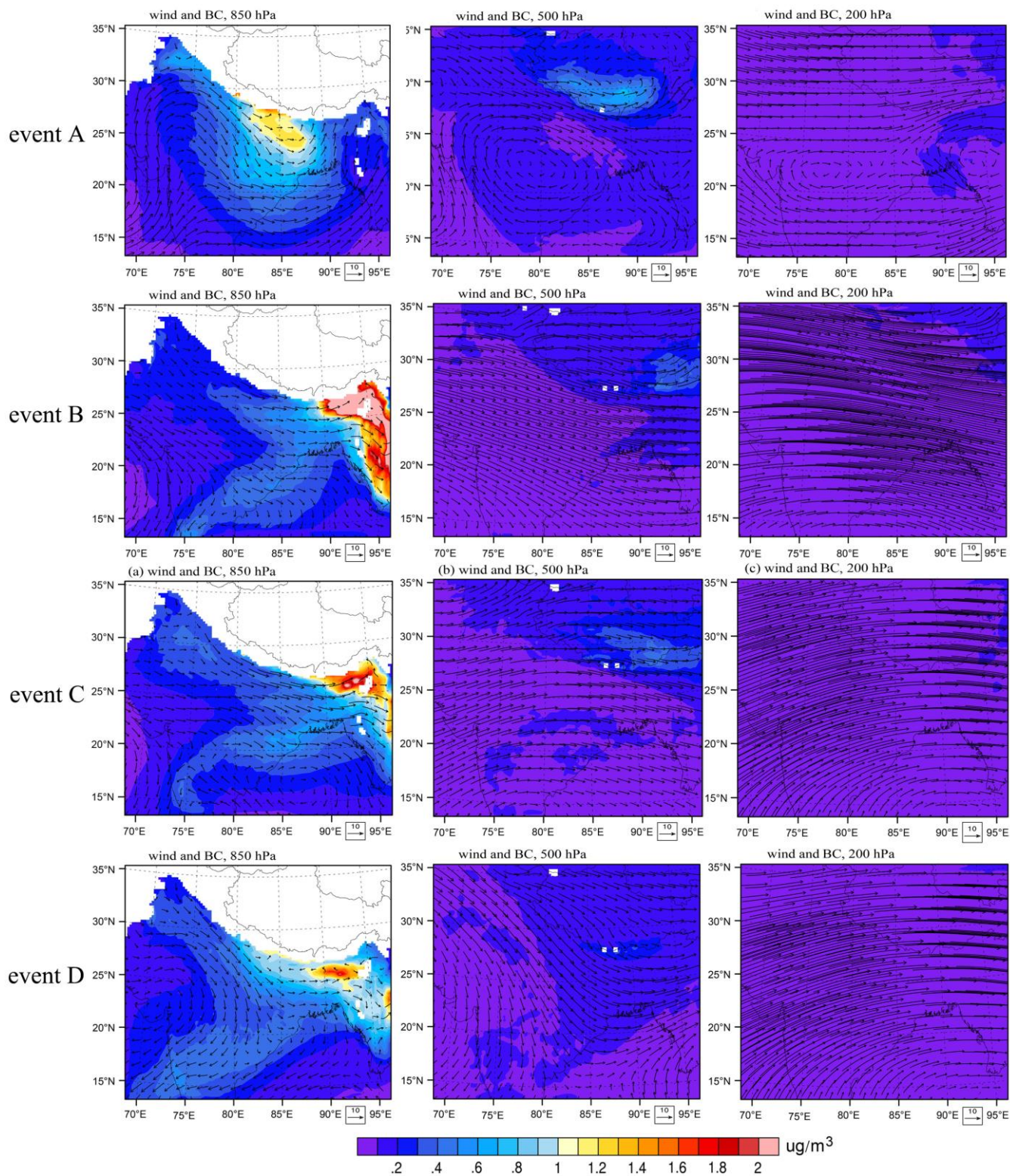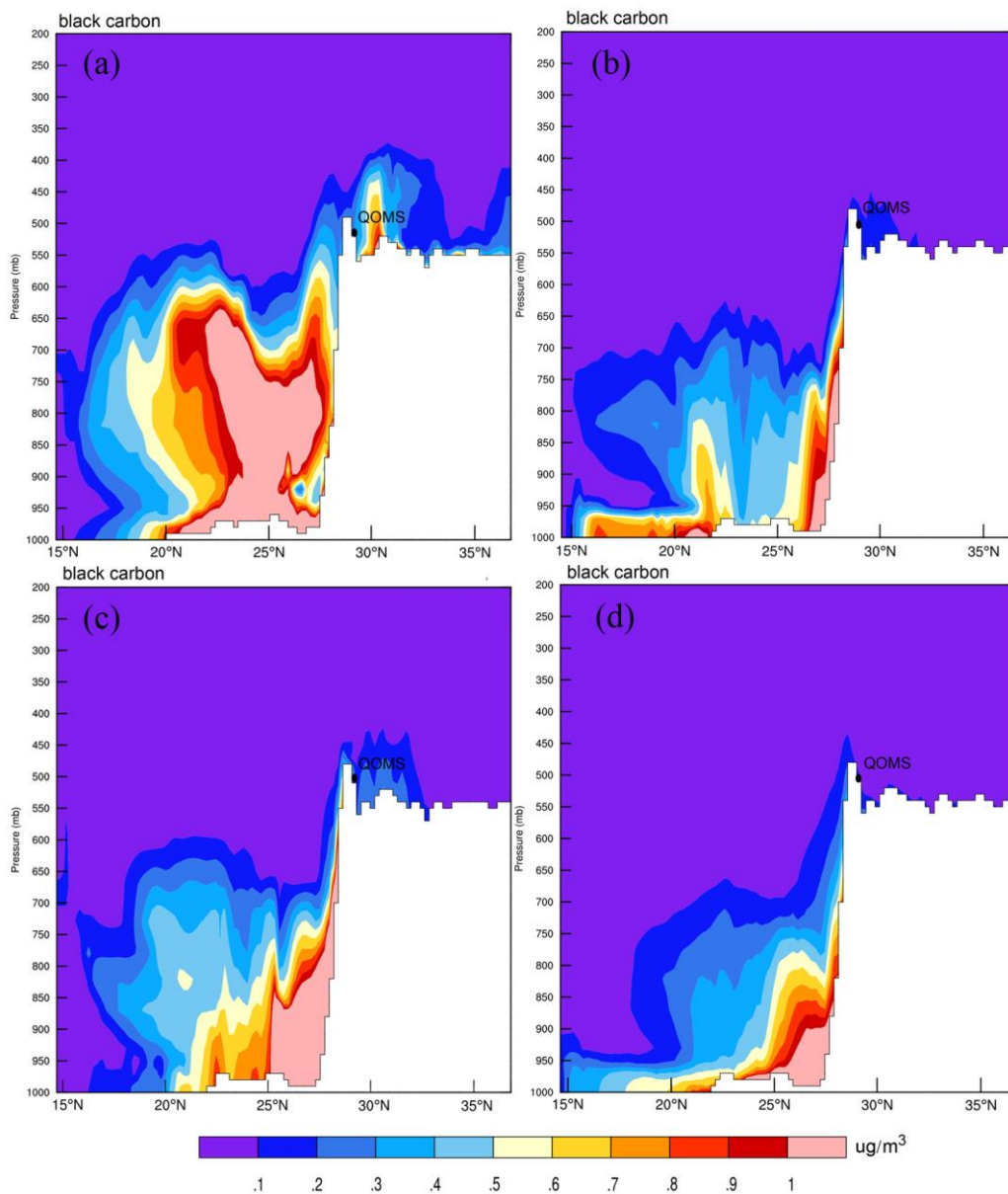
632

Figure 9. Mean BC concentration and wind at 850 hPa, 500 hPa, and 200 hPa simulated by WRF-Chem model at QOMS and its

vicinities: event A (the first row); event B (the second row); event C (the third row); event D (the last row).

635

636

Figure 10. **Vertical profiles of mean BC concentration along the QOMS's longitude of 86.95°E: (a) event A; (b) event B; (c) event C;**
(d) event D.

639

640

30